Open Ceramics 19 (2024) 100651

Contents lists available at ScienceDirect

Open Ceramics

journal homepage: www.sciencedirect.com/journal/open-ceramics

Residues from beneficiation of granite in porcelain stoneware: Effects on technological properties

Chiara Molinari [a,*], Andreea Sima [b], Matteo Cavina [c], Guia Guarini [a], Sonia Conte [a], Stefania Albonetti [c], Enrique Sanchez [b], Eugeni Cañas [b], Michele Dondi [a], Chiara Zanelli [a]

[a] Institute of Science, Technology and Sustainability for the development of Ceramic materials CNR-ISSMC, Via Granarolo, 64 48018, Faenza, RA, Italy
[b] Instituto Universitario de Tecnología Cerámica, Universidad Jaume I, Av. Vicente Sos Baynat s/n, 12006, Castellón, Spain
[c] Alma Mater Studiorum - Bologna University, Department of Industrial Chemistry "Toso Montanari" - Viale Risorgimento, 4, 40136, Bologna, Italy

ARTICLE INFO

Handling Editor: Dr P Colombo

Keywords:
Granite waste
Porcelain stoneware
Ceramic tiles

ABSTRACT

Granite extraction waste represents an interesting alternative material for porcelain stoneware production, but information on its influence presents several gaps. For this reason, two different wastes were selected: a coarser iron-rich material from magnetic separation and a finer one from conveyance and abatement systems. Both were physically and chemically characterized. Batches were formulated by partial substitution of feldspar and technological behaviour of bodies was assessed by simulating the industrial manufacture at laboratory scale. Tiles were shaped by uniaxial pressure and fired by fast firing in electric roller kiln. The effect of waste addition was evaluated during the whole production process. Fired samples were characterized in terms of technological properties, mineralogical composition and microstructure evolution. The formulation optimization reduces firing temperature getting commercial technological constraints. A further increase of finer waste content affects compaction and mechanical strength. The presence of micaceous particles after the firing process may act as cracks initiation.

1. Introduction

Granite rocks have long been exploited for a wide range of applications, including ornamental stone [1], quartz-feldspathic flux for vitrified ceramics [2–5], crushed aggregates for concrete and mortar [6,7], boulders and ballast for civil engineering [8,9].

Extraction and processing to achieve the technical specifications for the various uses of granite generate different kinds of waste [10]. Each of them has specific chemical and physical characteristics, which affect the possibility of recycling that can be expressed in terms of technology readiness level (TRL).

- Quarry residues are basically made of blocks that do meet the requirements for ornamental stone and fine-grained tails. The former waste is currently reused (TRL 9) as ceramic flux [11–14] or in civil engineering, e.g., as boulders for outer dam and breakwater in ports [15]. The fine-grained tails have been investigated as ceramic raw material as well [16].
- Residues of cutting, sawing and polishing operations on ornamental stone consist essentially of powdered granite, contaminated by grinding media and additives: the main issue is the increased values of Fe_2O_3, CaO and pH [17,18]. Attempts have been spent for the valorisation of these residues in ceramic products of various types, including clay bricks and roof tiles, wall and floor tiles and lightweight aggregates [19–24]. As far as we know, this waste is only occasionally used by the ceramic industry in red-body products, mainly bricks [25–28], while for whiteware the TRL is around 5–6.
- Fractions discarded by the beneficiation of quartz-feldspathic flux (mostly for porcelain stoneware tiles, but also glazes, sanitary ware and container glass) are typically composed of granite enriched in femic minerals, e.g., biotite, amphiboles, Fe-oxides [29–31]. The mineralurgical processes that are commonly used [32–35] are grinding and sieving (to achieve mineral liberation) and high field intensity magnetic separation or less frequently froth flotation (to achieve the separation of iron-bearing minerals). The resulting residues can be relatively coarse-grained (magnetic fraction) or fine-grained (flotation tailings, dust from air cleaning of the

* Corresponding author.
E-mail address: chiara.molinari@cnr.it (C. Molinari).

https://doi.org/10.1016/j.oceram.2024.100651
Received 26 June 2024; Received in revised form 31 July 2024; Accepted 31 July 2024
Available online 5 August 2024

treatment plant). As far as we know, the level of technological readiness for recycling these types of waste is low, probably around TRL 2.

In the processing of granites, to obtain 100,000 tons of feldspar product, the amount of waste generated is typically about 12 thousand tons of magnetic fraction and about 7 thousand tons of dust from air cleaning [13]. Considering that the world production of feldspar from granites is around 3.6 million tons per year [5], the global yearly output of residues can be approximately estimated at 250,000 tons (dust from air cleaning) and 430,000 tons (magnetic fraction).

While the recycling of residues from quarrying, sawing and polishing of ornamental granite has already been the subject of many studies, detailed investigation on the behaviour of beneficiation waste in the ceramic process is not available. To fill this gap, laboratory-scale experiments were carried out to reveal the technological behaviour of coarse-grained (magnetic fraction) and fine-grained (dust from air cleaning) residues in the manufacture of porcelain stoneware tiles.

The main limitation of the magnetic fraction is its high iron oxide content, which affects colour but can also cause aesthetic defects in ceramics, such as speckling and unwanted stains [30,36,37]. High iron levels have been ascribed for defects such as black core and bloating [38–40]. It is necessary to understand if there are technological constraints in the design of sustainable bodies, which can tolerate a darker colour or speckling, to be used in "green" tiles [41–43].

The problem with de-dusting waste is handling a very fine-grained powder, which is difficult to mix with the other ingredients of the batch and can affect compaction and drying operations, reducing the air permeability of compacts [44,45]. It would be useful to understand to what extent these drawbacks can be tolerated in novel sustainable batches for ceramic tiles [43,46].

The goal of the present study is to understand the reasons behind the behaviour of granite beneficiation waste and the defects that can be generated in the ceramic process to improve the chance of recycling.

2. Material and methods

Two types of waste, resulting from different steps of granite beneficiation for the production of feldspathic fluxes, were sampled at the Minerali Industriali Plant in Verbania, Italy. The granite under exploitation pertains to the Variscan Serie dei Laghi [47]. These samples are characterized by different properties and colour: the fraction discarded from high field intensity magnetic separation is dark-coloured (named SD) while dust collected at the filters for air cleaning is light-coloured (named SL). Both residues were evaluated in terms of feasibility as secondary raw materials for porcelain stoneware tiles.

The chemical composition of both raw materials and residues was determined by Energy Dispersive X-ray Fluorescence Spectrometry (EDS-XRF) with S2 PUMA (Bruker, Germany) and is reported in Table 1.

The mineralogical composition was investigated by X-ray Diffraction (D8 Advance with LynxEye 1-dimensional detector, Bruker, Germany) in the following conditions: 40 kV, 40 mA, radiation source Cu Kα ($\lambda = 0.154183$ nm) collecting data over a range of 2θ between 10^o and 100^o using a step size of 0.02^o. A quantitative determination of phase composition of fired bodies at optimal firing temperature was carried out by Rietveld refinement (GSAS-EXPGUI software), adding 20 % (by weight) of corundum as internal standard to estimate the vitreous phase by difference, that is 100 % minus the sum of crystalline phase [48]. The particle size distribution was measured by X-ray monitoring of gravity sedimentation (ASTM C958–92:2022 by Sedigraph 5100, Micromeritics, UK) [49]. Fusibility of waste materials was tested by hot-stage microscopy (ODP868, TA, Germany) up to melting (heating rate 10 °C/min). Characteristic temperatures (end of sintering, softening, bloating, sphere, hemisphere, melting) were determined with an experimental uncertainty of ±5 °C [50].

The residues under investigation were added to a typical porcelain stoneware formulation (named R) in place of sodium feldspar. Three different waste contents were selected (up to 9 % by weight): batch formulations are reported in Table 2.

The tile-making process was replicated in laboratory. All the raw materials underwent a preliminary grinding by jaw crusher and hammer mill (2 mm grid) before mixing. The batches (2 kg each) were wet ground for 25 min in planetary mill (porcelain jar and alumina grinding media, 40 wt% water, 0.4 wt %sodium tripolyphosphate). The slips were oven dried (105 °C overnight) then pulverized in hammer mill (grid 0.5 mm). Powders were hand granulated (8 % wt/wt moisture) through a 2 mm sieve. Tiles of 11 cm × 5.5 cm x 0.5 cm were shaped by uniaxial pressure (40 MPa) with a hydraulic press, then dried (105 °C overnight). The industrial process was simulated by fast firing in electric roller kiln at maximum temperature in the 1180–1230 °C range (60 min cold-to-cold). The following technological properties were determined: green and dry bulk density (mass/volume); pressing spring back (100*(green sample length – mould length)/mould length); drying shrinkage (100*(green sample length – dry sample length green sample length); green, dry and fired modulus of rupture [51], firing shrinkage [52], fired bulk density and water absorption [53]. The microstructure of the fired specimens at maximum densification was observed by scanning electron microscopy (FE-SEM, Zeiss Sigma, Carl Zeiss, Germany). Moreover, energy–dispersive X–ray microanalysis (EDX) was employed with the aim of determining the elemental distribution in different zones of the fired specimens. Through an X-ray spectrometer and an energy detector

Table 2
Porcelain stoneware formulations (wt%).

Batch	R	SD3	SD6	SD9	SL3	SL6	SL9
Clays (50/50 wt% HP/LP)	40	40	40	40	40	40	40
Quartz-feldspathic sand QS	15	15	15	15	15	15	15
Sodium feldspar NF	45	42	39	36	42	39	36
Granite waste SD (magnetic fraction)	/	3	6	9	/	/	/
Granite waste SL (air cleaning dust)	/	/	/	/	3	6	9

Table 1
Chemical composition of raw materials (wt%).

Material	Dark-coloured granite waste (magnetic fraction)	Light-coloured granite waste (air cleaning dust)	High plasticity ball clay	Low plasticity ball clay	Sodium feldspar	Quartz-feldspathic sand
Code	SD	SL	HP	LP	NF	QS
SiO_2	70.3	71.7	60.0	58.1	70.4	79.6
TiO_2	0.8	0.2	1.6	1.6	0.3	0.1
Al_2O_3	12.0	15.5	26.1	27.0	17.9	9.0
Fe_2O_3	6.1	2.0	1.0	0.9	0.1	0.8
MgO	0.8	0.2	0.6	0.6	0.1	0.3
CaO	1.4	1.3	0.4	0.4	0.7	2.5
Na_2O	2.4	3.5	0.5	0.5	9.7	1.9
K_2O	5.0	4.7	2.6	2.6	0.3	3.2
L.o.I.	1.2	0.9	7.2	7.4	0.3	2.6
Total	100.0	100.0	100.0	100.0	100.0	100.0

(Genesis 7000 SUTW, EDAX, USA) several spectra were taken at low vacuum and 20 kV under the backscattering electrons signal. Colourimetric parameters were measured by a portable spectrophotometer (MiniScan XE Plus, Hunterlab, USA) directly on fired tiles to achieve L*, a* and b* coordinates [54] together with the chroma value C* by the following equation: $C^* = \sqrt{(a^*)^2+(b^*)^2}$. The colour difference was calculated with respect to the reference body (L_R^*, a_R^*, b_R^*) by the equation: $\Delta E^* = \sqrt{(L^* - L_R^*)^2 + (a^* - a_R^*)^2 + (b^* - b_R^*)^2}$.

3. Results and discussion

3.1. Properties of waste materials and batches

The X-ray patterns of SD and SL samples are reported in Fig. 1. Both residues consist of quartz, feldspars, chlorite and biotite, in accordance with the mineralogical composition of the granite excavated [55,56]. The dark-coloured waste SD, however, contains a higher amount of biotite and chlorite, which are the iron-bearing minerals enriched by magnetic separation into the discarded fraction.

The chemical and mineralogical similitudes are reflected in firing behaviour, as appreciable from the fusibility test (Fig. 2). The rather high content of iron oxide found in SL, and particularly in SD, improves the fusibility of granite, as expected [36,50,57]. Indeed, the characteristic temperatures of residues are close to those of a strong flux like sodium feldspar (Table 3). On the other hand, the clear bloating phenomenon, with strong expansion of SD and SL specimens between the softening and sphere stages, is a well-known effect of iron oxide in fluxes [5,58].

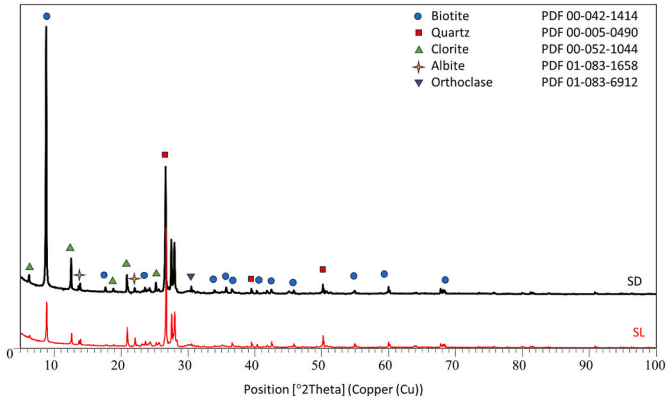

Fig. 1. X-ray patterns of SD and SL granite residues.

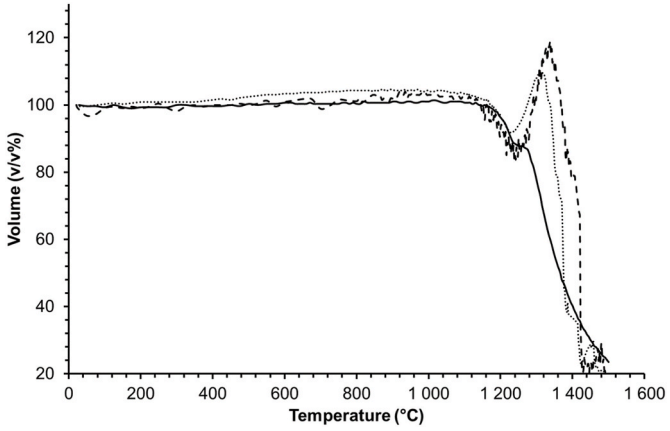

Fig. 2. Hot-stage microscopy analysis of the two waste materials (SL dotted line; SD dashed line) compared to the sodium feldspar NF (full line).

Table 3
Characteristic temperatures and bloating behaviour.

Characteristic temperature (°C)	Magnetic fraction SD	Air cleaning dust SL	Sodium feldspar NF
End of sintering	1226	1234	1220
Softening	1250	1272	1265
Bloating	1314	1338	1270
Sphere	1334	1358	1315
Hemisphere	1372	1420	1365
Melting	1418	1424	1450
Maximum expansion (%)	110	119	84

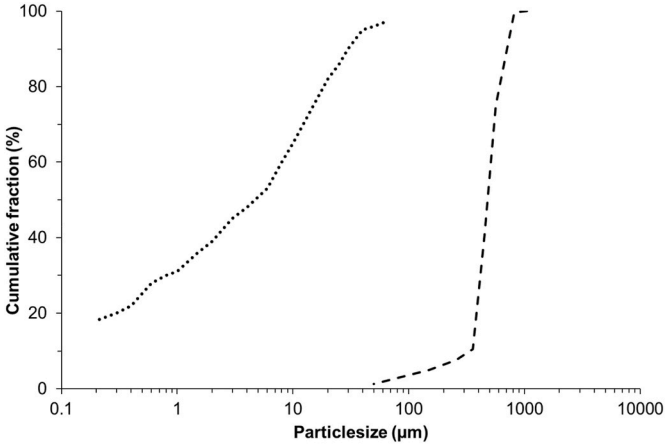

Fig. 3. Particle size distribution of granite residues (SL dotted line; SD dashed line).

In terms of particle size, the materials show different distributions, derived by the process involved in their production (Fig. 3). In particular, the dark-coloured waste is characterized by coarser particles, with D_{100} and D_{50} of 800 µm and 450 µm, respectively (Fig. 3). The light-coloured residue shows a particle size distribution shifted to lower values, having 70 wt% of particles smaller than 63 µm and values of D_{100} and D_{50} of 250 µm and 150 µm, respectively.

3.2. Technological properties of porcelain stoneware batches

After milling, all batches show comparable results in terms of particle size distribution (Fig. 4). In fact, differences between the various slips fall within the uncertainty of measurement. These distributions fulfil the granulometric range of industrial porcelain stoneware [59].

The technological behaviour of both green and dry tiles was not significantly affected by waste addition (Table 4). All properties exhibit values in line with the reference ones and any variation is within the standard deviation of measurements.

3.3. Technological properties of fired specimens: granite waste from magnetic separation (SD)

Gresification curves (linear shrinkage, bulk density, and water absorption as a function of firing temperature) are reported in Fig. 5 for the different batches under study. Reference body shows an increasing shrinkage till 1220 °C, at which corresponds a water absorption complying to the standard requirement for porcelain stoneware tiles (<0.5 % according to ISO 13006, Group BIa) [60] and a bulk density as high as 2.37 g cm^{-3}. The SD addition promoted sintering phenomena (as already found by Il'ina and Lebedeva, 2010) [36] and allowed an increased densification for additions of 6–9% waste. A reduction of the maximum densification temperature occurred already for 3 % waste, and a temperature decrease of 20 °C was registered for 9 % waste. The maximum densification was in all cases achieved for water absorption

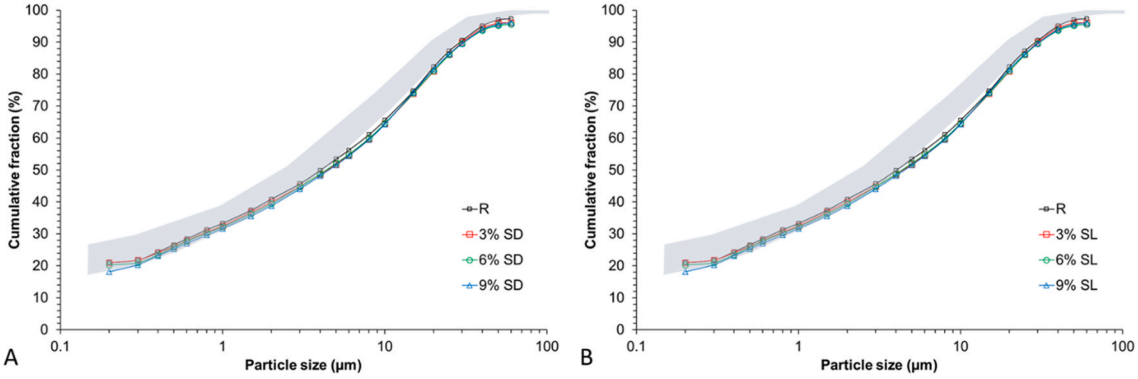

Fig. 4. Particle size distribution of slips with reference to the granulometric range of porcelain stoneware bodies (grey field). Effect of waste amount for A) magnetic fraction SD; B) air cleaning dust SL.

Table 4
Technological behaviour of green and dry tiles.

Variable	Pressing springback	Green bending strength	Green bulk density	Drying shrinkage	Dry bending strength	Dry bulk density
Batch	cm/m	MPa	kg/m^3	cm/m	MPa	kg/m^3
R	0.45 ± 0.03	1.0 ± 0.1	2.13 ± 0.02	0.06 ± 0.01	3.2 ± 0.2	1.98 ± 0.02
SD3	0.43 ± 0.02	1.1 ± 0.1	2.14 ± 0.02	0.04 ± 0.02	3.1 ± 0.2	1.99 ± 0.01
SD6	0.48 ± 0.02	1.0 ± 0.1	2.13 ± 0.02	0.06 ± 0.01	3.0 ± 0.2	1.98 ± 0.02
SD9	0.45 ± 0.01	1.0 ± 0.1	2.15 ± 0.01	0.05 ± 0.01	3.1 ± 0.1	1.98 ± 002
SL3	0.47 ± 0.01	1.0 ± 0.1	2.14 ± 0.01	0.04 ± 0.01	3.4 ± 0.2	2.00 ± 0.01
SL6	0.45 ± 0.03	0.9 ± 0.1	2.11 ± 0.01	0.05 ± 0.02	3.0 ± 0.6	1.98 ± 0.02
SL9	0.46 ± 0.03	1.1 ± 0.1	2.13 ± 0.02	0.05 ± 0.02	3.2 ± 0.1	2.00 ± 0.02

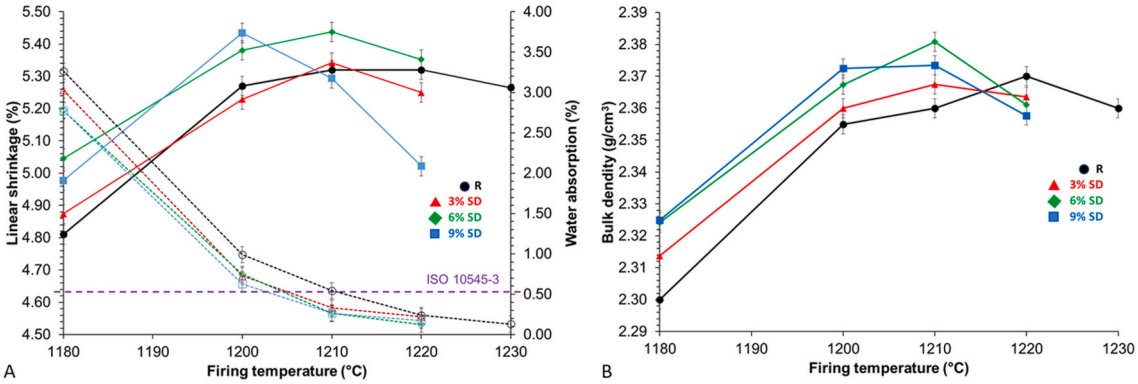

Fig. 5. Gresification curves of bodies containing the dark-coloured granite waste from magnetic separation: A) linear shrinkage and water absorption, and B) bulk density as a function of firing temperature.

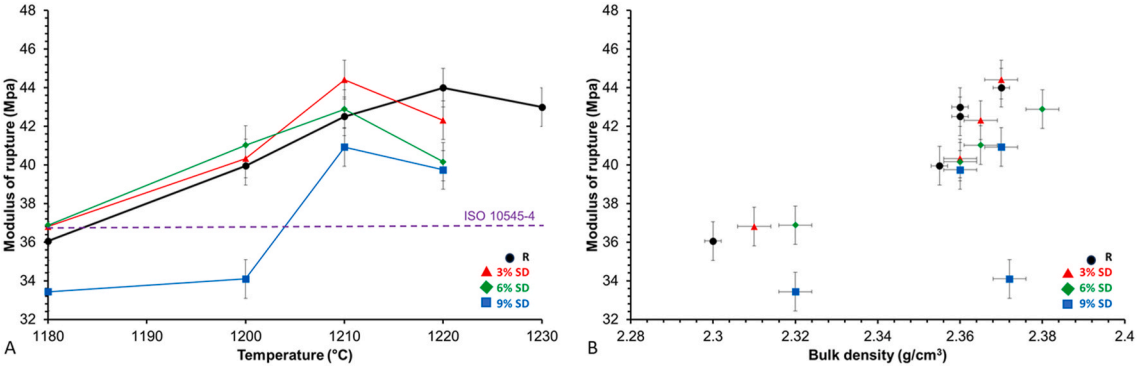

Fig. 6. Mechanical properties of the reference body compared to SD waste-based ones: modulus of rupture as a function of firing temperature (A) and bulk density (B).

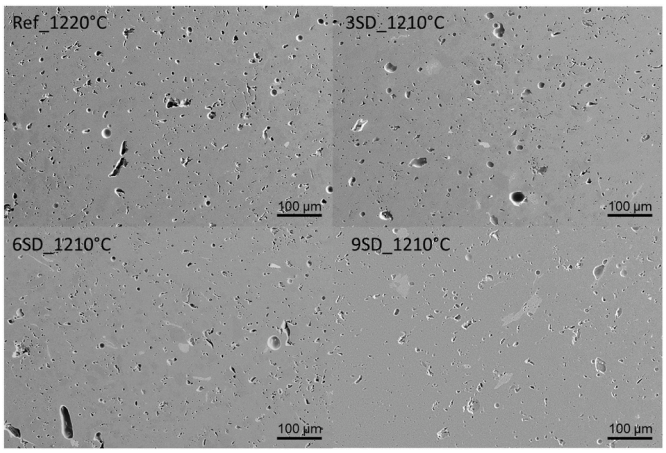

Fig. 7. Microstructure of porcelain stoneware bodies with increasing content of SD waste at maximum densification temperature.

lower than 0.5 %, so no clue emerged of anticipated overfiring [61]. However, the body expansion due to overfiring was more pronounced in all the SD containing samples. In fact, the dimensional stability at high temperature (calculated from gresification curves as the thermal interval in which the linear shrinkage is within ±0.05 % of the maximum value) is broad for the reference body (30 °C) but distinctly shorter in presence of waste (10–14 °C for 3–6% of SD addition and only 6 °C for 9 % SD).

The different firing behaviours above discussed reflects on the mechanical properties (Fig. 6). Regardless the bulk density achieved during the firing process, the measured modulus of rupture decreased with the addition of granite waste. In particular, the batch containing 9 % of SD suffered from an important loss of mechanical strength. The reason behind this detrimental effect must be searched in the microstructure of fired specimens.

Comparing bodies fired at the maximum densification temperature, typical microstructural features of porcelain stoneware can be observed (Fig. 7): irregular pores (up to 150 μm) that derives from defects of powder compaction along with rounded pores (diameter between 20 and 5 μm) that are the residual fraction left by gas trapping and pore coalescence [62]. In accordance with the gresification curves, the occurrence of waste favoured the sintering process: the porosity observed in micrographs is decreasing from R to 9SD, with less frequent larger pores.

The most interesting aspect that can explain the mechanical resistance is the microstructural heterogeneity furtherly introduced by waste addition. Looking in detail, solid particles occur in the waste-bearing bodies, as irregular fragments, light grey in colour, up to 200 μm in size (Fig. 7). They are remnants of the original dark-coloured grains in the SD waste, consisting of biotite-chlorite that were decomposed during the firing process. However, both the layered structure and the chemical signature of biotite are still preserved (Fig. 8). Similar features were found in ceramic bodies containing the magnetic fraction of alkali syenite [36] or raw granite [29]. These remnants probably play as microstructural defects, promoting crack initiation under lower stress [63,64], and so reducing the whole mechanical resistance of porcelain stoneware tiles [65–67].

All the batches fired at the temperature of maximum densification are characterized by a similar phase composition, consisting of a high

Table 5
Phase composition at the temperature of maximum densification.

Batch	R	SD3	SD6	SD9
Optimal firing temperature (°C)	1220	1210	1210	1210
wt%				
Quartz	24.1 ± 0.5	23.4 ± 0.1	23.5 ± 0.4	23.9 ± 0.1
Mullite	8.2 ± 0.3	8.0 ± 0.1	7.8 ± 0.3	8.2 ± 0.3
Plagioclase	4.0 ± 0.1	4.0 ± 0.1	3.8 ± 0.4	2.6 ± 0.1
K-Feldspar	1.2 ± 0.1	1.2 ± 0.1	1.0 ± 0.1	0.4 ± 0.1
Vitreous Phase	62.5 ± 1.0	63.4 ± 0.4	63.6 ± 1.2	64.9 ± 0.6

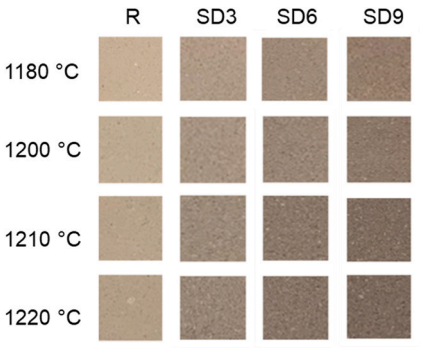

Fig. 9. Effect of waste content and firing temperature in colour aspect of fired samples.

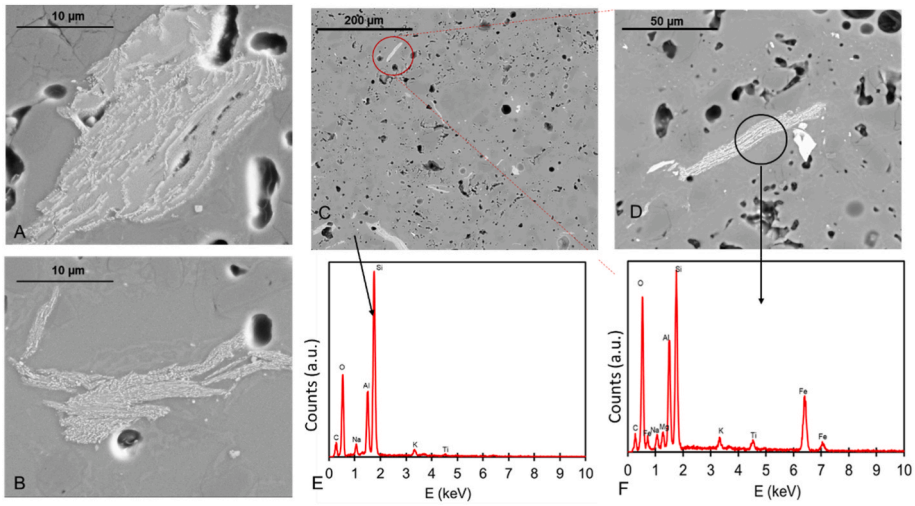

Fig. 8. Microstructural properties of 6 wt% SD samples at maximum densification; A-D) microstructure details and E-F) EDS elemental composition.

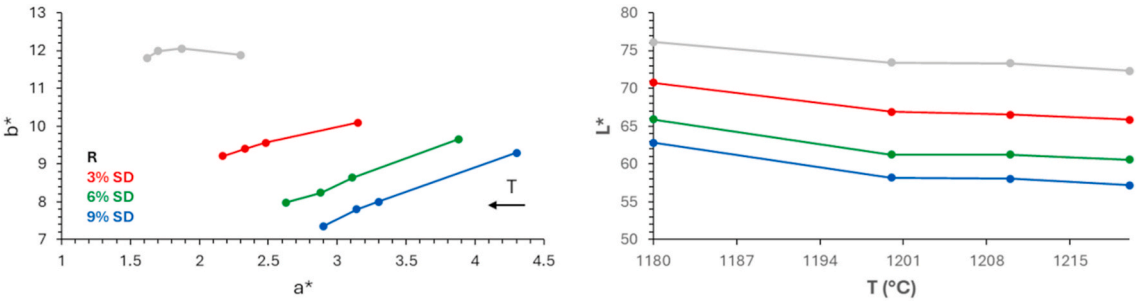

Fig. 10. L*, a* and b* coordinates measured for SD containing samples.

Table 6
Colorimetric parameters of specimens fired at optimal firing temperature.

Batch	R	SD3	SD6	SD9
Optimal firing temperature (°C)	1220	1210	1210	1210
L*	72.3 ± 0.2	66.5 ± 0.1	61.2 ± 0.3	58.0 ± 0.4
a*	1.62 ± 0.03	2.33 ± 0.05	2.88 ± 0.04	3.14 ± 0.04
b*	11.81 ± 0.10	9.40 ± 0.06	8.24 ± 0.06	7.80 ± 0.18
C*	11.92 ± 0.11	9.68 ± 0.08	8.73 ± 0.09	8.40 ± 0.12
ΔE*		6.3 ± 0.3	11.7 ± 0.3	14.9 ± 0.6

amount of vitreous phase embedding mullite, quartz and feldspars (Table 5). These compositions are fully comparable with those of commercial porcelain stoneware tiles [68–70].

Going in detail, the amount of feldspars is slightly decreasing (and the vitreous phase is slightly increasing) by increasing the waste addition. Nevertheless, the addition of waste instead of sodium feldspar implies a different mineralogical composition of SD-bearing batches, which are poorer in plagioclase (from 4 % in SD3 to 2.6 % in SD9) compared to the benchmark. However, differences in the feldspar amount are smaller in the fired bodies than in the raw batches, and this let to suppose that the waste addition made feldspars slightly more stable.

Although no diffractometric evidence of biotite or chlorite emerged in the fired bodies, we can argue from SEM observations that their iron content did not diffuse completely into the glassy phase, but largely remained limited to the biotite remnants. Analogous observations have been reported for ceramics containing granite residues [20,29]. This fact has an impact on the colorimetric parameters and the appearance of the fired bodies, which turn to be less and less homogeneous in colour as the waste amount increased (Figs. 9 and 10).

Increasing the waste percentage led, as expected, to a progressive darkening of the bodies, enhanced by firing temperature. For specimens fired at optimal firing temperature, a relevant drop of L* (from 72 to 58) and rise of ΔE* (from 6.32 to 14.91) is observed, not reflected in the C* values that are surprisingly decreasing (Table 6). This occurred because the yellow coordinate b* decreased, while the red coordinate a* slightly increased. The non-linear dependence of the colour coordinates on the SD additions is probably due to various factors, which could not be quantified, such as the presence of iron oxide in localized spots (biotite residues) or diffused in the vitreous phase [29,69]. The fact that not all the iron oxide, added as waste SD, has diffused in the vitreous phase can explain the firing behaviour, which is not affected by dimensional instability and bloating to the extent that could have been foreseen based on the iron content of the batch [5,71,72].

3.4. Technological properties of fired specimens: granite dust from air cleaning (SL)

The presence of the dust from the aspiration system (SL) had a different effect on gresification curves compared to the magnetic fraction SD. The impact on the temperature of maximum densification or that at which water absorption fulfils the standard requirement (<0.5 w/w%) is modest, being at most 10 °C below the reference body (Fig. 11). Another repercussion of waste addition consists in a slightly increased firing shrinkage, despite that the bulk density of dry tiles was substantially the same. This may be explained by the slightly greater bulk density of SL3 and SL6 fired tiles with respect to the benchmark, with a shift of the maximum densification from 1220 to 1200 °C. However, the observed behaviour does not scale with the waste content: in case of 6SL, both firing shrinkage and water absorption are higher than 3SL and 9SL.

An unusual trend for the mechanical properties was observed: the addition of 3 % SL improved the modulus of rupture up to the

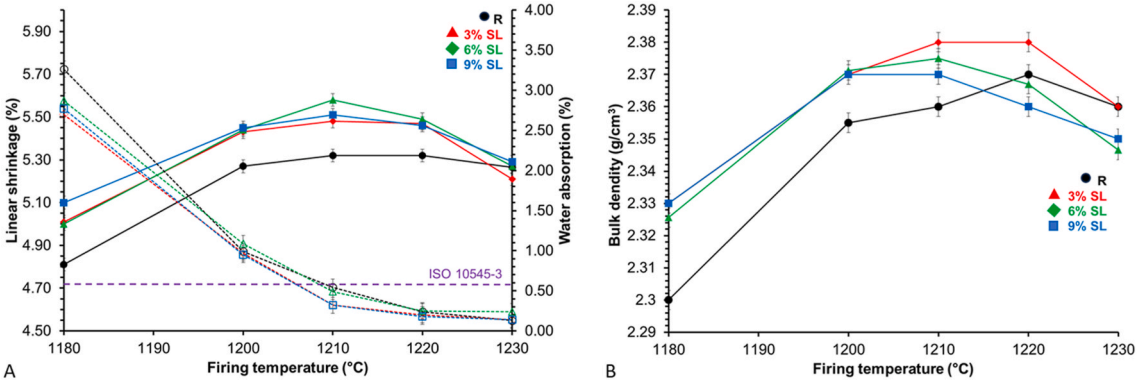

Fig. 11. Gresification curves of bodies containing the light-coloured granite dust from air cleaning (SL): A) linear shrinkage and water absorption, and B) bulk density as a function of firing temperature.

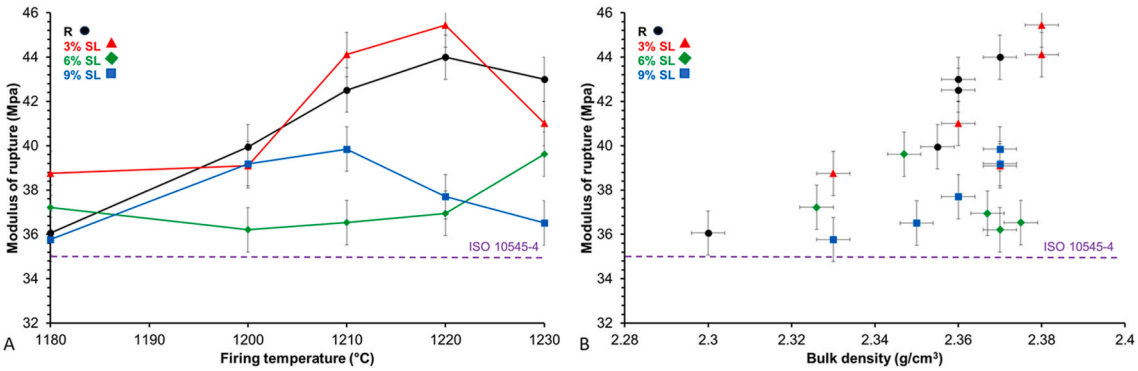

Fig. 12. Mechanical properties of the reference body compared to SL waste-based ones: modulus of rupture as a function of firing temperature (A) and bulk density (B).

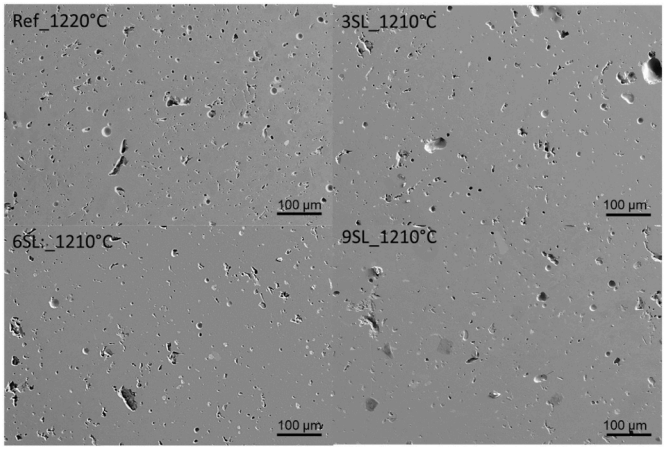

Fig. 13. Microstructure evolution with light waste content at maximum densification temperature.

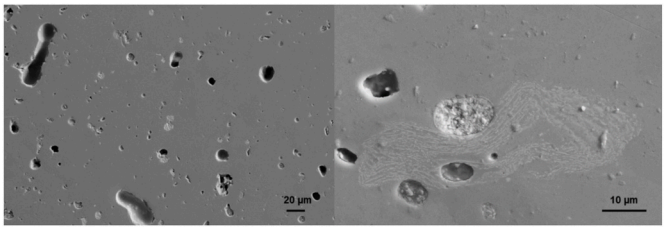

Fig. 14. Microstructural details of 6 wt% SL sample at optimal firing temperature.

temperature of maximum densification. The further temperature rise led to a drop in the modulus below that of the reference body (Fig. 12). When the waste content was increased, the behaviour changed completely and a clear loss of mechanical performance as a function of firing temperature can be observed for SL6 and SL9, with no apparent relation with the reference material. Anyway, all the evaluated samples match the minimum requirement of standard ISO 13006.

Similarly, to the SD-based bodies, the reason of the mechanical performance can be found in the microstructural properties [63] that are shown in Fig. 13 for the samples fired at optimal temperature. The addition of waste favoured the sintering process, reducing number and size of pores, in agreement with the finer particle size of SL. At the same time, the presence of spherical aggregates formed by finer particles can be observed (Fig. 14). In the case of SL6, it is possible to see a larger number of aggregates with respect to the other waste-based samples.

Table 7
Phase composition at the optimal firing temperature.

Batch	R	SL3	SL6	SL9
Optimal firing temperature (°C)	1220	1210	1210	1210
Quartz	24.1 ± 0.5	23.2 ± 0.4	23.5 ± 0.3	24.3 ± 0.3
Mullite	8.2 ± 0.3	8.1 ± 0.3	8.2 ± 0.1	8.2 ± 0.3
Plagioclase	4.0 ± 0.1	3.9 ± 0.1	3.4 ± 0.4	3.2 ± 0.1
K-Feldspar	1.2 ± 0.1	1.2 ± 0.1	0.6 ± 0.1	0.4 ± 0.1
Vitreous Phase	62.5 ± 0.1	63.6 ± 0.4	64.3 ± 0.9	63.9 ± 0.1

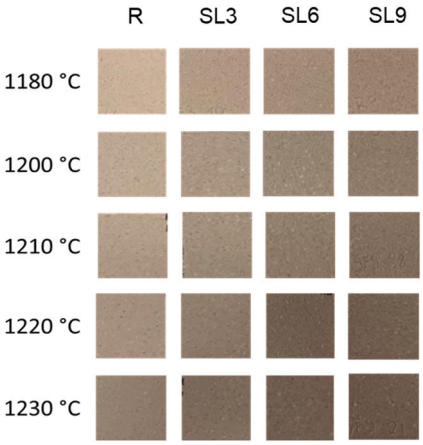

Fig. 15. Effect of waste content and firing temperature in colour aspect of fired samples.

Despite all batches were prepared following the same procedure, the technological properties change non-linearly, making not easily predictable the effect of SL addition.

The batches fired at the temperature of maximum densification are characterized by a similar phase composition, with amount of vitreous phase higher than 62 % together with mullite, quartz and feldspars (Table 7) and fully comparable with commercial porcelain stoneware [68,70].

Also in the case of SL, the addition of waste led to a darkening of the colour of tiles (Figs. 15 and 16) due to the progressive dissolution of chromophores into the melt, enhanced by temperature increase [29] and the slightly larger percentage of vitreous phase [69].

Colour changed as a function of SL addition, less than the SD-bearing bodies, with L* decreasing (from 72 to 66) associated to a slight reduction of the yellow coordinate b* and a slight increase of the red

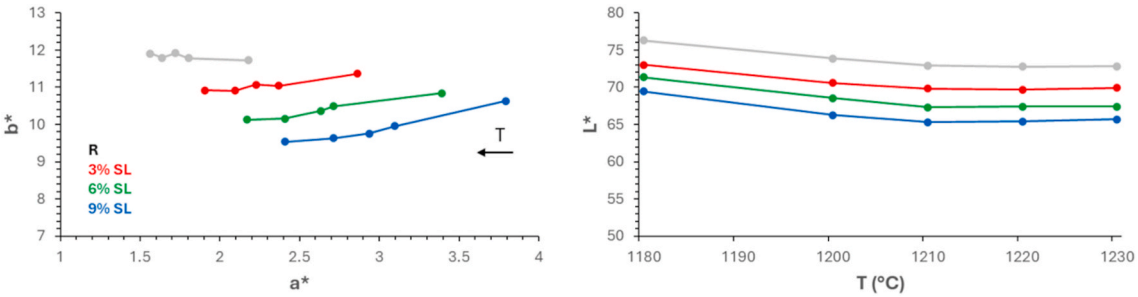

Fig. 16. L*, a* and b* coordinates measured for SL containing samples.

Table 8
Colorimetric parameters of specimens fired at optimal firing temperature.

Batch	R	SL3	SL6	SL9
Firing temperature (°C)	1220	1210	1210	1210
L*	72.3 ± 0.2	70.6 ± 0.5	68.5 ± 0.1	66.3 ± 0.1
a*	1.62 ± 0.03	2.37 ± 0.13	2.71 ± 0.05	3.79 ± 0.04
b*	11.81 ± 0.10	11.04 ± 0.18	10.48 ± 0.05	9.96 ± 0.12
C*	11.92 ± 0.11	11.29 ± 0.08	10.83 ± 0.12	10.43 ± 0.09
ΔE*		3.1 ± 0.4	5.8 ± 0.2	7.9 ± 0.2

coordinate a* (Table 8).

4. Conclusions

The present study has investigated the reasons behind the defects occurring in the production of porcelain stoneware tiles when granite residues (magnetic fraction and dust from aspiration system) are used. Although these materials are in principle compatible with porcelain stoneware batches, their use in partial replacement of sodium feldspar induced technical and aesthetic drawbacks (darker colour, speckling, loss of mechanical strength) together with limited advantages (reduction in the optimal firing temperature of 10 °C). Not all the iron oxide added by the magnetic fraction diffused in the vitreous phase formed during firing. This had pros (less dimensional instability and bloating than expectable based on the iron content of the batch) and cons (unesthetic spots made of biotite remnants). On the other hand, the introduction of discontinuity elements into the matrix affects the mechanical strength in two different ways. In the case of SD, the presence of micrometric irregular particles may act as cracks initiator under flexural tests, reducing the mechanical properties regardless the higher bulk densification of the whole material. In this case, a further particle size reduction may help to reduce this phenomenon and improving sintering. For the dust from aspiration system, the origin of defects is more complex. The tendency of fines to remain aggregated lead to the formation of low compact elements that reduce the breakdown strength. At the same time, the dispersion of dusts into the slurry during wet mill is not even controllable without the addition of additives, avoiding the possibility to predict final properties. In this case, an accurate tuning of rheological properties is mandatory.

CRediT authorship contribution statement

Chiara Molinari: Writing – review & editing, Writing – original draft, Project administration, Formal analysis, Data curation, Conceptualization. **Andreea Sima:** Writing – review & editing, Formal analysis. **Matteo Cavina:** Formal analysis. **Guia Guarini:** Formal analysis. **Sonia Conte:** Formal analysis. **Stefania Albonetti:** Supervision. **Enrique Sanchez:** Writing – review & editing, Supervision. **Eugeni Cañas:** Formal analysis. **Michele Dondi:** Writing – review & editing, Supervision, Conceptualization. **Chiara Zanelli:** Writing – review & editing.

Acknowledgements

Project funded under the National Recovery and Resilience Plan (NRRP), Mission 04 Component 2 Investment 1.5-NextGenerationEU, Call for tender n. 3277 dated December 30, 2021 Award Number: 0001052 dated June 23, 2022.

Authors from ITC acknowledge grant from EDGJID – 2021 program of the Generalitat Valenciana.

Authors greatly thank Minerali Industriali S.r.l., in particular Alberto Cazzaniga and Stefano Di Primio, for materials supply.

References

[1] P.M. Amaral, J.C. Fernandes, V. Pires, L.G. Rosa, Ornamental stones, in: M. C. Gonçalves, M. Margarido (Eds.), Materials for Construction and Civil Engineering: Science, Processing, and Design, Springer, 2015, pp. 397–445, https://doi.org/10.1007/978-3-319-08236-3.
[2] C. Fiori, B. Fabbri, Granite-containing bodies for the production of stoneware tiles, Interceram 32 (1983) 21–22.
[3] M.I. Ryshchenko, L.P. Shchukina, E.Y. Fedorenko, K.N. Firsov, Possibility of obtaining ceramogranite using quartz-feldspar raw material from Ukraine, Glass Ceram. 65 (2008) 23–26, https://doi.org/10.1007/s10717-008-9011-8.
[4] H.F. El-Maghraby, M.M. El-Omla, F. Bondioli, S.M. Naga, Granite as flux in stoneware tile manufacturing, J. Am. Ceram. Soc. 31 (2011) 2057–2063, https://doi.org/10.1016/j.jeurceramsoc.2011.05.023.
[5] M. Dondi, G. Guarini, S. Conte, C. Molinari, R. Soldati, C. Zanelli, Deposits, composition and technological behavior of fluxes for ceramic tiles, Period. Mineral. 88 (2019) 235–257, https://doi.org/10.2451/2019PM861.
[6] H. Binici, T. Shah, O. Aksogan, H. Kaplan, Durability of concrete made with granite and marble as recycle aggregates, J. Mater. Process. Technol. 208 (2008) 299–308, https://doi.org/10.1016/j.jmatprotec.2007.12.120.
[7] R.A. Hamza, S. El-Haggar, S. Khedr, Marble and granite waste: characterization and utilization in concrete bricks, Int. J. Biosci. Biochem. Bioinforma. 1 (2011) 286–291.
[8] C. Brown, Construction, maintenance and monitoring of Plymouth breakwater, J. Coast Res. 65 (2013) 165–170, https://doi.org/10.2112/SI65-029.1.
[9] Y. Guo, J. Xie, Z. Fan, V. Markine, D.P. Connolly, G. Jing, Railway ballast material selection and evaluation: a review, Construct. Build. Mater. 344 (2022) 128218, https://doi.org/10.1016/j.conbuildmat.2022.128218.
[10] E. Lewicka, Rational use of selected mining by-products in the ceramic industry in Poland, Gospodarka Surowcami Mineralnymi-Mineral Resources Management 36 (2020) 59–76, https://doi.org/10.24425/gsm.2020.132547.
[11] G. Bozzola, P. Danasino, S. Di Primio, Recycling of granite processing waste for feldspar production, Fourth European Ceramic Society Conf. Proc. 11 (1995) 19–26.
[12] G.A. Dino, M. Fornaro, A. Trentin, Quarry waste: chances of a possible economic and environmental valorisation of the Montorfano and Baveno granite disposal sites, J. Geol. Res. 2012 (2012) 11, https://doi.org/10.1155/2012/452950.
[13] G.A. Dino, A. Cavallo, P. Rossetti, E. Garamvölgyi, R. Sándor, F. Coulon, Towards sustainable mining: exploiting raw materials from extractive waste facilities, Sustainability 12 (2020) 2383, https://doi.org/10.3390/su12062383.
[14] M.V. Vasić, N. Mijatović, Z. Radojević, Aplitic granite waste as raw material for the production of outdoor ceramic floor tiles, Materials 15 (2022) 3145, https://doi.org/10.3390/ma15093145.
[15] S.K. Nayak, A. Satapathy, S. Mantry, Use of waste marble and granite dust in structural applications: a review, J. Build. Eng. 46 (2022) 103742, https://doi.org/10.1016/j.jobe.2021.103742.
[16] D. Tonnayopas, K. Kooptarnond, M. Masae, Novel ecological tiles made with granite fine quarry waste and oil palm fiber ash, Sci. Technol. Aliment. 1 (2009) 10–20.

[17] V. Barrientos, J. Delgado, V. Navarro, R. Juncosa, I. Falcón, A. Vázquez, Characterization and geochemical–geotechnical properties of granite sawdust produced by the dimension stone industry of O Porriño (Pontevedra, Spain), Q. J. Eng. Geol. Hydrogeol. 43 (2012) 141–155, https://doi.org/10.1144/1470-9236/08-098.

[18] M.C. Aguiar, M.C.B. Gadioli, M.P. Babisk, V.S. Candido, N.S. Monteiro, C.M. F. Vieira, Characterization of a granite waste for clay ceramic addition, Mater. Sci. Forum 775 (2014) 699–704. https://doi.org/10.4028/www.scientific.net/MSF.775-776.699.

[19] P. Torres, H.R. Fernandes, S. Agathopoulos, D.U. Tulyaganov, J.M.F. Ferreira, Incorporation of granite cutting sludge in industrial porcelain tile formulations, J. Eur. Ceram. Soc. 24 (2004) 3177–3185, https://doi.org/10.1016/j.jeurceramsoc.2003.10.039.

[20] C.M.F. Vieira, S.N. Monteiro, Incorporation of granite waste into vitrified ceramic tiles, Mater. Sci. Forum 530 (2006) 467–472. https://doi.org/10.4028/www.scientific.net/MSF.530-531.467.

[21] R.R. Menezes, H.M. Neto, L.N.L. Santana, H.L. Lira, H.S. Ferreira, G.A. Neves, Optimization of wastes content in ceramic tiles using statistical design of mixture experiments, J. Eur. Ceram. Soc. 28 (2008) 3027–3039, https://doi.org/10.1016/j.jeurceramsoc.2008.05.007.

[22] A.J. Souza, B.C.A. Pinheiro, J.N.F. Holanda, Processing of floor tiles bearing ornamental rock-cutting waste, J. Mater. Process. Technol. 210 (2010) 1898–1904, https://doi.org/10.1016/j.jmatprotec.2010.07.001.

[23] M. Hojamberdiev, A. Eminov, Y. Xu, Utilization of muscovite granite waste in the manufacture of ceramic tiles, Ceram. Int. 37 (2011) 871–876, https://doi.org/10.1016/j.ceramint.2010.10.032.

[24] B. Ngayakamo, A. Bello, A.P. Onwualu, Valorization of granite waste powder as a secondary flux material for sustainable production of ceramic tiles, Clean. Mater. 4 (2022) 100055, https://doi.org/10.1016/j.clema.2022.100055.

[25] S.N. Monteiro, L.A. Peçanha, C.M.F. Vieira, Reformulation of roofing tiles body with addition of granite waste from sawing operations, J. Eur. Ceram. Soc. 24 (2004) 2349–2356, https://doi.org/10.1016/S0955-2219(03)00638-1.

[26] P. Torres, R.S. Manjate, S. Quaresma, H.R. Fernandes, J.M.F. Ferreira, Development of ceramic floor tile compositions based on quartzite and granite sludges, J. Eur. Ceram. Soc. 27 (2007) 4649–4655, https://doi.org/10.1016/j.jeurceramsoc.2007.02.217.

[27] W. Acchar, K.A. Avelino, A.M. Segadães, Granite waste and coffee husk ash synergistic effect on clay-based ceramics, Adv. Appl. Ceram. 115 (2016) 236–242, https://doi.org/10.1080/17436753.2015.1126989.

[28] A.J. Araújo, A.R. Sousa, D.A. Macedo, R.P. Dutra, L.F. Campos, Effects of granite waste addition on the technological properties of industrial silicate based-ceramics, Mater. Res. Express 6 (2020) 125205, https://doi.org/10.1088/2053-1591/ab62e8.

[29] E. Lewicka, Phase transitions of ferruginous minerals in the course of thermal processing of feldspar-quartz raw materials from the Sobótka region (Lower Silesia), Gospodarka Surowcami Mineralnymi-Mineral Resources Management 33 (2017) 93–110, https://doi.org/10.1515/gospo-2017-0010.

[30] N. Rowson, P. Fears, Magnetic properties of ceramic minerals, Interceram 6 (2020) 16–19.

[31] T. Vrbický, R. Přikryl, Recovery of some critical raw materials from processing waste of feldspar ore related to hydrothermally altered granite: laboratory-scale beneficiation, Minerals 11 (2021) 455, https://doi.org/10.3390/min11050455.

[32] M. Agus, R. Angius, M. Ghiani, R. Peretti, A. Serci, A. Zucca, Beneficiation of low grade feldspar ores for the ceramics industry, Dev. Chem. Eng. Miner. Process. 13 (2000), https://doi.org/10.1016/S0167-4528(00)80087-3. C11-17-C11-25.

[33] M. El-Omla, S. Shata, Recovery of feldspar raw material from granite rocks for ceramic and porcelain industries, Geol. Resour. 17 (2008) 235–240, https://doi.org/10.13686/j.cnki.dzyzy.2008.03.006.

[34] A.I. Ismail, D.S. Ghabrial, W.A. Wahab, M. Eissa, A. Cazzaniga, C. Zanelli, M. Dondi, Exploring syenites from ring complexes in the Eastern Desert (Egypt) as ceramic raw materials, Period. Mineral. 87 (2018) 67–81, https://doi.org/10.2451/2018PM749.

[35] M.F. Raslan, S. Kharbish, M.M. Fawzy, M.M. El Dabe, M.M. Fathy, Gravity and magnetic separation of polymetallic pegmatite from wadi el sheih granite, central eastern desert, Egypt, J. Min. Sci. 57 (2021) 316–326, https://doi.org/10.1134/S1062739121020162.

[36] V.P. Il'ina, G.A. Lebedeva, Use of wastes from concentration of alkali syenites from the Elet'ozerskoe deposit for manufacture of ceramic tiles, Glass Ceram. 67 (2010) 99–202, https://doi.org/10.1007/s10717-010-9262-z.

[37] M. Carlini, S. Castellucci, E. Allegrini, B. Giannone, S. Ferrelli, E. Quadraroli, D. Marcantoni, M.T. Saurini, Ceramic flaws: laboratory tests and analysis using Scanning Electron Microscope to identify surface defects, J. Eur. Ceram. Soc. 34 (2014) 2655–2662, https://doi.org/10.1016/j.jeurceramsoc.2014.01.009.

[38] K.J.D. MacKenzie, C.M. Cardile, A 57 Fe Mössbauer study of black coring phenomena in clay-based ceramic materials, J. Mater. Sci. 25 (1990) 2937–2942, https://doi.org/10.1007/BF00584908.

[39] G. Ferrari, P. Zannini, C. Baraldi, Study of Black Core, ceramic tile's defect, by a multi technique approach. ICORS 2014-XXIV International Congress on Raman Spectroscopy Proceedings, 2014.

[40] M.G. Moshnyakov, V.Z. Abdrakhimov, Investigations of the black core and swelling in firing porcelain stoneware, Glass Ceram. 76 (2019) 270–273, https://doi.org/10.1007/s10717-019-00181-8.

[41] E. Rambaldi, S. Fazio, F. Prete, M.C. Bignozzi, Innovative ceramic tile mixes: 100% green, cft-Ber. DKG 93 (2016) E57–E60.

[42] E. Rambaldi, Pathway towards a high recycling content in traditional ceramics, Cerâmica 4 (2021) 486–501, https://doi.org/10.3390/ceramics4030036.

[43] J. Castellano, V. Sanz, E. Canas, E. Sánchez, Industry-scalable wall tile composition based on circular economy, Bol. Soc. Espanola Ceram. Vidr. 61 (2022) 374–382, https://doi.org/10.1016/j.bsecv.2022.03.003.

[44] J.S. Reed, From batch to pressed tile: mechanics and system microstructural changes. QUALICER 6th World Congress on Ceramic Tile Quality, Spain, Proceedings, 2000, pp. 23–42.

[45] J.L. Amorós, M.J. Orts, J. García-Ten, A. Gozalbo, E. Sánchez, Effect of the green porous texture on porcelain tile properties, J. Eur. Ceram. Soc. 27 (2007) 2295–2301, https://doi.org/10.1016/j.jeurceramsoc.2006.07.005.

[46] C. Zanelli, S. Conte, C. Molinari, R. Soldati, M. Dondi, Waste recycling in ceramic tiles: a technological outlook, Resour. Conserv. Recycl. 168 (2021) 105289, https://doi.org/10.1016/j.resconrec.2020.105289.

[47] A. Boriani, L. Burlini, V. Caironi, E. Giobbi Origoni, A. Sassi, E. Sesana, Geological and petrological studies on the hercynian plutonism of Serie dei Laghi–geological map of its occurrence between Valsesia and Lago Maggiore (N-Italy), Rend. Soc. It. Mineral. Petrol 43 (1988) 367–384.

[48] A.F. Gualtieri, V. Riva, A. Bresciani, S. Maretti, M. Tamburini, A. Viani, Accuracy in quantitative phase analysis of mixtures with large amorphous contents. The case of stoneware ceramics and bricks, J. Appl. Crystallogr. 47 (2014) 835–846.

[49] ASTM C958-92, Standard Test Method for Particle Size Distribution of Alumina or Quartz by X-Ray Monitoring of Gravity Sedimentation, 2022.

[50] M. Dondi, G. Guarini, I. Venturi, Assessing the fusibility of feldspathic fluxes for ceramic tiles by hot stage microscope, Ind. Ceram. 21 (2001) 67–73.

[51] ISO 10545-4, Ceramic Tiles - Part 4: Determination of Modulus of Rupture and Breaking Strength, 2019.

[52] ASTM C326-09, Standard Test Method for Drying and Firing Shrinkages of Ceramic Whiteware Clays, 2018.

[53] ISO 10545-3, Ceramic Tiles - Part 3: Determination of Water Absorption, Apparent Porosity, Apparent Relative Density and Bulk Density, 2018.

[54] ISO 10545-16, Ceramic Tiles – Part 16: Determination of Small Colour Differences, 2010.

[55] V. Caironi, R. Bocchio, L. Ottolini, Biotiti e cloriti nelle diverse facies del granito di Baveno-Mottarone (Verbania), Plinius 32 (2006) 363–364.

[56] G. Bozzola, A. Lorenzi, G.A. Dino, M. Fornaro, Innovazioni tecnologiche, alternative e materie prime seconde dalla gestione virtuosa degli scarti e dei rifiuti dell'attività estrattiva. L'esempio virtuoso del Gruppo Minerali Maffei S.p.A, in: A. Giuliani, V. Baldino, P. Lattanzi (Eds.), Rocce e minerali industriali, Aracne, Roma, 2011, pp. 119–141. ISBN: 8854837458.

[57] E. Lewicka, Z. Ociepa, P. Wyszomirski, Possibilities of beneficiation of the feldspar-quartz rock from Sławniowice near Nysa in the light of so-far research, Gospodarka Surowcami Mineralnymi – Mineral Resources Management 23 (2007) 5–19, in Polish.

[58] M. Dondi, P. Cappelletti, M. D'Amore, R. de Gennaro, S.F. Graziano, A. langella, M. Raimondo, C. Zanelli, Lightweight aggregates from waste materials: reappraisal of expansion behavior and prediction schemes for bloating, Construct. Build. Mater. 127 (2016) 394–409, https://doi.org/10.1016/j.conbuildmat.2016.09.111.

[59] S. Conte, C. Zanelli, C. Molinari, G. Guarini, M. Dondi, Glassy wastes as feldspar substitutes in porcelain stoneware tiles: thermal behaviour and effect on sintering process, Mater. Chem. Phys. 256 (2020) 123613, https://doi.org/10.1016/j.matchemphys.2020.123613.

[60] ISO 13006, Ceramic Tiles. Definitions, Classification, Characteristics and Marking, 2018.

[61] F. Contartesi, F. Gomes Melchiades, A. Ortega Boschi, Anticipated Overfiring in Porcelain Tiles: effects of the firing cycle and green bulk density, Bol. Soc. Espanola Ceram. Vidr. 58 (2019) 69–76, https://doi.org/10.1016/j.bsecv.2018.07.001.

[62] C. Molinari, Y. Alaya, L. Pasti, G. Guarini, M. Dondi, C. Zanelli, Assessing white clays from Tabarka (Tunisia) in the production of porcelain stoneware tiles, Appl. Clay Sci. 231 (2023) 106741, https://doi.org/10.1016/j.clay.2022.106741.

[63] C. Leonelli, F. Bondioli, P. Veronesi, M. Romagnoli, T. Manfredini, G.C. Pellacani, V. Cannillo, Enhancing the mechanical properties of porcelain stoneware tiles: a microstructural approach, J. Eur. Ceram. Soc. 21 (2001) 785–793, https://doi.org/10.1016/S0955-2219(00)00266-1.

[64] T.L. Anderson, Fracture Mecahanics. Fundamentals and Applications, fourth ed., CRC Press, Taylor&Francis Group, Boca Raton, 2017 https://doi.org/10.1201/9781315370293.

[65] A. De Noni Jr., D. Hotza, V.C. Soler, E.S. Vilches, Influence of composition on mechanical behaviour of porcelain tile. Part II: mechanical properties and microscopic residual stress, Mater. Sci. Eng. 527 (2010) 1736–1743, https://doi.org/10.1016/j.msea.2009.10.060.

[66] J. Martín-Márquez, J.M. Rincón, M. Romero, Effect of microstructure on mechanical properties of porcelain stoneware, J. Eur. Ceram. Soc. 30 (2010) 3063–3069, https://doi.org/10.1016/j.jeurceramsoc.2010.07.015.

[67] M. Romero, J.M. Pérez, Relation between the microstructure and technological properties of porcelain stoneware. A review, Mater. Construcción 65 (2015), https://doi.org/10.3989/mc.2015.05915 e065-e065.

[68] A. De Noni Jr., D. Hotza, V.C. Soler, E.S. Vilches, Influence of composition on mechanical behaviour of porcelain tile. Part I: microstructural characterization and

developed phases after firing, Mater. Sci. Eng. 527 (2010) 1730–1735, https://doi.org/10.1016/j.msea.2009.10.057.
[69] M. Lassinantti Gualtieri, M. Romagnoli, A.F. Gualtieri, Influence of body composition on the technological properties and mineralogy of stoneware: a DOE and mineralogical–microstructural study, J. Eur. Ceram. Soc. 31 (2011) 673–685, https://doi.org/10.1016/j.jeurceramsoc.2010.12.002.
[70] C. Zanelli, M. Raimondo, G. Guarini, M. Dondi, The vitreous phase of porcelain stoneware: composition, evolution during sintering and physical properties, J. Non-Cryst. Solids 357 (2011) 3251–3260, https://doi.org/10.1016/j.jnoncrysol.2011.05.020.
[71] G.P. Souza, P.F. Messer, W.E. Lee, Effect of varying quartz particle size and firing atmosphere on densification of Brazilian clay-based stoneware, J. Am. Ceram. Soc. 89 (2006) 1993–2002, https://doi.org/10.1111/j.1551-2916.2006.00986.x.
[72] S. Mestre, M.P. Gómez-Tena, M.F. Gazulla, A. Gozalbo, Interaction of the chromium–iron black pigment with porcelanised stoneware, Ceram. Int. 39 (2013) 7453–7459, https://doi.org/10.1016/j.ceramint.2013.02.090.